Electric-field poling of silicon nitride waveguides for the linear phase modulation

Boris Zabelich[a], Edgars Nitiss[a], Anton Stroganov[b], and Camille-Sophie Brès[a,*]

[a]Photonic Systems Laboratory (PHOSL), Ecole Polytechnique Fédérale de Lausanne, STI-IEM, Lausanne, Switzerland
[b]LIGENTEC SA, EPFL Innovation Park, Ecublens, Switzerland

ABSTRACT

Stoichiometric silicon nitride (Si_3N_4) constitutes a mature platform for integrated photonics. Its pertinent properties, including wide transparency window from the visible to the mid-IR, low propagation loss, and high third-order nonlinearity, are exploited in many linear and nonlinear applications. However, due to the centrosymmetric nature of the Si_3N_4, the absence of the second-order susceptibility ($\chi^{(2)}$) impedes a realization of three-wave mixing processes as well as the linear electro-optic effect, relevant for many applications on an optical chip. Here, we implement the electric-field poling technique to induce the effective $\chi^{(2)}$ inside a Si_3N_4 waveguide, thus enabling the linear electro-optic modulation. Using numerical simulations, we estimated the concentration and the diffusion coefficient of the charges responsible for the space-charge electric field formation. In addition, the DC third-order susceptibility of Si_3N_4 previously unknown in the literature is measured using a free-space Mach-Zehnder interferometer.

Keywords: Silicon nitride, phase modulator, electric-field poling, electro-optic effect

1. INTRODUCTION

Stoichiometric silicon nitride (Si_3N_4) is one of the highly studied platforms for linear and nonlinear light control at the micrometre-scale. Properties of the material, such as its large transparency window from visible to mid-infrared region, high refractive index, and relatively high third-order nonlinearity, are exploited in many applications. The latter is key to Kerr comb generation,[1] supercontinuum generation,[2] generation of non-classical states of light,[3] and others. However, in dipole approximation, the second-order nonlinear response is hindered in Si_3N_4 due to its centrosymmetric structure. The linear phase modulation of light and three-wave-mixing processes (e.g., second-harmonic generation (SHG)) based on second-order susceptibility $\chi^{(2)}$ are, however, essential parts of on-chip optical functionality.

Scientific interest has been focused on circumventing this constraint in centrosymmetric materials. For instance, to induce an effective $\chi^{(2)}$ in silicon waveguides, a silicon nitride film can be deposited on top to create symmetry breaking at the core-cladding interface.[4] It was recently shown that in this approach, the second-order nonlinear response originates due to the formation of the charged layers and, therefore, the electric field at the boundary of two materials.[5] The DC field E_{DC} acts on the third-order susceptibility $\chi^{(3)}$ to induce an effective $\chi^{(2)}_{\mathrm{eff}}$:

$$\chi^{(2)}_{\mathrm{eff}} = 3\chi^{(3)} E_{\mathrm{DC}} \tag{1}$$

Second-order susceptibility can be also induced using the formation of the space-charge separation region in Si_3N_4 waveguides via all-optical poling (AOP).[6–8] In the AOP technique, the coherent photogalvanic effect leads to the charge separation in a periodic manner due to the absorption interference of a fundamental-harmonic pump and its second-harmonic.[9,10] The inscribed nonlinear grating spontaneously satisfies the quasi-phase-matching (QPM) condition for the interacting light beams resulting in the rapid conversion efficiency increase of SHG. The latter demonstrations clearly indicate that the movement of ionic charge carriers is taking place inside the Si_3N_4 optical waveguide. Yet, despite the efforts, the understanding of charge carrier properties, such as their

*Corresponding author: camille.bres@epfl.ch

concentration and mobility, is still limited. Thermally assisted electric-field poling is an alternative method for the inscription of an electric field within a waveguiding medium and could provide means for enabling studies of charge carrier properties in the optical waveguides as well as pave the way for novel $\chi^{(2)}$-based applications. The thermally assisted electric-field poling technique utilizes the fact that the charges present in the material immobile at room temperature, can be thermally activated ($\approx 300°$C), and then displaced by an externally applied field.[11,12] The sample is cooled down to room temperature with the electric field still applied, fixing the charges in their new positions. The inscribed DC field can be used for the linear electro-optic modulation.[13] The refractive index change Δn with respect to the applied electric field E_0 in materials lacking second-order susceptibility is described by:

$$\Delta n = \frac{3\chi^{(3)}E_0^2}{2n_0} \tag{2}$$

where n_0 is the unperturbed refractive index of a material. The applied electric field can comprise DC E_{DC} and sinusoidal components E_{m} at the modulation frequency ω_{m}:

$$E_0 = E_{\mathrm{DC}} + E_{\mathrm{m}} sin(\omega_{\mathrm{m}} t) \tag{3}$$

Expanding the term E_0^2 in eq. 2, it is evident that the refractive index change has several frequency components: at DC, ω_{m}, and $2\omega_{\mathrm{m}}$. The amplitudes of the induced refractive index at ω_{m} and $2\omega_{\mathrm{m}}$ are given, respectively, by:

$$\Delta n_{\omega} = \frac{3\chi^{(3)}}{n_0} E_{\mathrm{DC}} E_{\mathrm{m}} \tag{4}$$

$$\Delta n_{2\omega} = \frac{3\chi^{(3)}}{4n_0} E_{\mathrm{m}}^2 \tag{5}$$

The dispersion of $\chi^{(3)}$ is expected to be negligible for the modulation frequency below tens of kilohertz. The static electric field can be either externally applied or inscribed within a waveguide. Eq. 4 describes the linear electro-optic effect with respect to modulation field amplitude at ω_{m}.

In this work, we demonstrate thermally assisted electric-field poling in Si_3N_4 waveguides enabled by the movable charges inside the material. We show that the amplitude of the refractive index change depends on the profiles of the interacting fields and, therefore, on the waveguide cross-section. Additionally, using numerical simulations of the charge movement during electric-field poling, we extract the charge carrier concentration and diffusivity coefficient. Finally, we measure the DC Kerr susceptibility of Si_3N_4 previously unknown in the literature.

2. RESULTS

2.1 Measurement of Si_3N_4 DC Kerr susceptibility

A Mach-Zehnder interferometer was used (Fig. 1(a)) for measuring the induced refractive index change in the Si_3N_4 optical waveguides. A TE polarized laser beam ($\lambda = 1560$ nm) is divided into two arms. The light in the signal arm is coupled in a waveguide for the phase modulation. The out-coupled light from the waveguide is combined with the beam from the reference arm, and both are directed to a photodetector. In the optical path of the reference arm, we place a glass wedge on a translation stage that provides means for the control of the relative phase difference between light in both arms. For the phase modulation, an amplified electric signal is applied on the electrodes integrated on the chip along the optical waveguide. A lock-in amplifier was used for precise phase change detection at ω_{m} and $2\omega_{\mathrm{m}}$ frequencies. The measurements were conducted at the modulation frequency of 5 kHz. Two waveguides with 1.31×0.81 μm^2 (referred in the text as *wide*) and 0.57×0.81 μm^2 (referred as *narrow*) cross-sections were studied (Fig. 1(b)). The integrated electrodes are placed in plane 10 μm apart from each other and 1.7 μm above a waveguide. The interacting lengths are 4.5 cm and 8.3 cm, for the wide and narrow waveguide, respectively.

In Fig. 1(d-g), the simulated distribution of the TE polarized optical mode and the externally applied electric field (in case 400 V between the electrodes) in both waveguides are shown. The simulation was done using

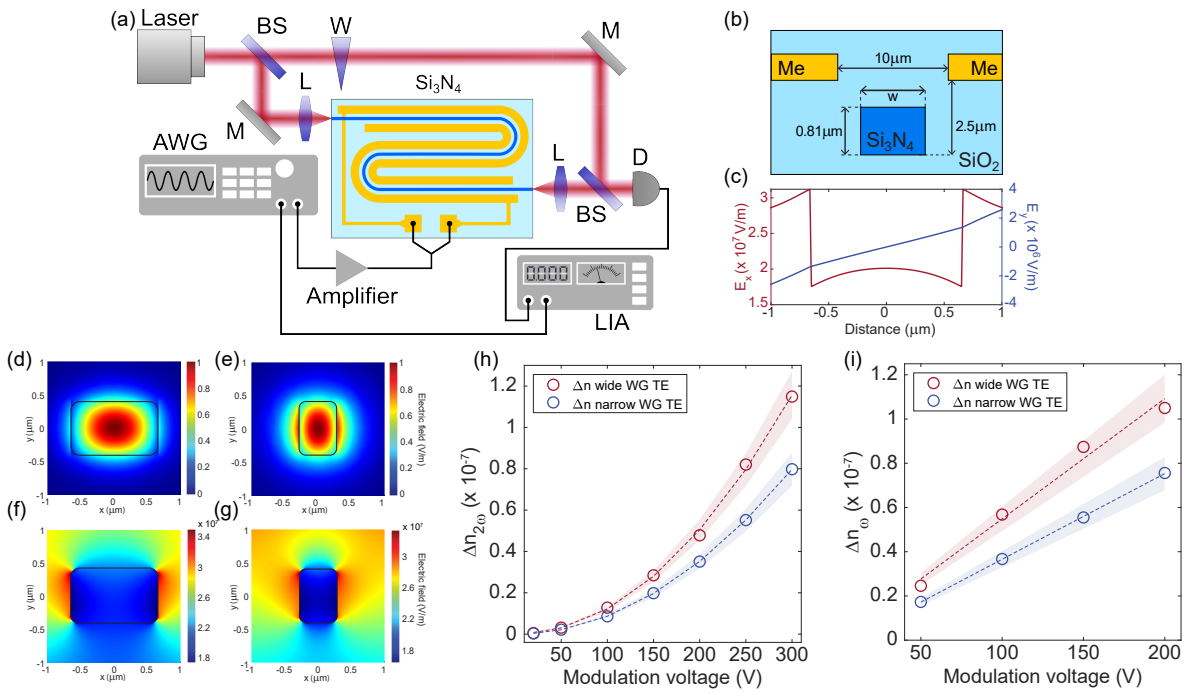

Figure 1. (a) Schematic of the interferometric set-up for the phase change detection. BS: beam splitter, L: lens, AWG: arbitrary waveform generator, W: optical wedge, M: mirror, D: detector, LIA: lock-in amplifier. (b) Device cross-section comprising Si_3N_4 waveguide core, silica cladding and metal electrodes. (c) Horizontal (E_x) and vertical (E_y) components of the externally applied electric field across the waveguide core with 1.31×0.81 μm^2 cross-section. (d, e) TE optical mode ($\lambda = 1560$ nm) and (f, g) externally applied electric field (400 V) distributions in waveguides with 1.31×0.81 μm^2 and 0.57×0.81 μm^2 cross-sections. (h, i) Refractive index change in the quadratic regime and the linear regime (under $V_{DC} = 100$ V) as a function of the modulation voltage amplitude, respectively.

COMSOL Multiphysics software, setting dielectric constants of silica and Si_3N_4 to be 4.2 and 7.5, respectively.[14] It is important to note that the spatial distribution of the applied electric field is independent of the applied voltage. Here the electric field is not uniformly distributed within the waveguiding medium, and the induced Δn_{eff} is determined by the overlap integral:[15]

$$\Delta n_{\text{eff}} = 2c\epsilon_0 \frac{\iint \Delta n(x,y)|\mathbf{E}(x,y)|^2 \, dxdy}{\iint (\mathbf{E}^* \times \mathbf{H} + \mathbf{E} \times \mathbf{H}^*)\hat{\mathbf{z}} \, dxdy} \tag{6}$$

where $\mathbf{E}$ and $\mathbf{H}$ are the electric and magnetic fields of the mode, respectively, propagating in the z-direction. The integral is calculated over the entire waveguide cross-section. By carrying the integration over the core and cladding regions, it is possible to find the contribution of each area solely and to derive the $\chi^{(3)}$ value of Si_3N_4. It is important to note that the applied electric field lies in the waveguide predominantly across the x-axis (Fig. 1(c)), allowing consideration of only the component of $\chi^{(3)}$ related to the light polarization parallel to the applied electric field. We first study unpoled optical waveguides. In Fig. 1(h,i), the induced refractive index change as a function of the modulation voltage amplitude in the quadratic and linear regimes is demonstrated. To enable the linear electro-optic modulation in this experiment, DC voltage of $V_{DC} = 100$ V was applied between the electrodes. The induced Δn for the modulation voltage of $V_{mod} = 100$ V for the linear (LEO) and quadratic electro-optic (QEO) effect in both waveguides are shown in Table 1.

The induced Δn is higher in the wide waveguide due to the larger overlap of the optical mode and electric field inside Si_3N_4, which is expected to have higher $\chi^{(3)}$ than silica cladding. As predicted by eq.4 and eq.5, the refractive index change measured in the linear regime is four times larger than that in the quadratic regime for the same DC and modulation voltage amplitudes. The value of silica $\chi^{(3)}(SiO_2) = 2\times10^{-22}$ pm/V was used to

Table 1. Refractive index change in the linear (Δn_ω) and quadratic ($\Delta n_{2\omega}$) regimes normalized for equal DC and modulation voltage amplitudes $V_{DC} = V_{mod} = 100$ V in the wide and narrow waveguides.

Cross-section	Δn_ω (LEO)	$\Delta n_{2\omega}$ (QEO)
$1.31 \times 0.81\ \mu m^2$	5.4×10^{-8}	1.3×10^{-8}
$0.57 \times 0.81\ \mu m^2$	3.8×10^{-8}	0.86×10^{-8}

calculate the cladding contribution to the total refractive index change via eq. 6. Finally, the value of Si_3N_4 can be derived to be $\chi^{(3)}(Si_3N_4) = 1.4\times10^{-21}$ pm/V. The measured third-order susceptibility of Si_3N_4 is one order magnitude larger than $\chi^{(3)}$ of silica as expected.[16] However, the obtained value is slightly less than $\chi^{(3)}(Si_3N_4)$ measured by optical means, e.g., optical Kerr effect.[17]

2.2 Thermally assisted electric field poling of Si_3N_4 waveguides

After the measurement of $\chi^{(3)}$ of Si_3N_4, the second-order nonlinearity was induced using thermally assisted electric field poling. The chip was kept on a ceramic plate at a temperature of 260°C while applying a DC voltage of 400 V across the sample. Each waveguide was subjected to poling procedures in several consecutive time steps followed by the measurement of the linear electro-optic response. Figure 2(a) shows the refractive index change normalized for $V_m = 1$ V during poling Δn^p_ω. The growth of Δn^p_ω saturates after several tens of minutes of poling. In contrast to poling of silica fibers, where for longer poling times the injection of hydrogenated species was observed leading to a reduction of $\chi^{(2)}_{eff}$,[12,18] the induced Δn^p_ω keeps the same value after 3 hours of poling, indicating that only one type of charges is involved in the process. Two-photon microscopy (TPM) was used to image the position of the inscribed electric field after electric-field poling.[8] During a raster-scan, the second-harmonic signal of a 1010 nm pump is collected across a sample. The received signal is proportional to the effective $\chi^{(2)}$. Figure 2(b) shows an optical photograph of the TPM studied area of the narrow waveguide, while Fig. 2(c) shows the TPM image. The signal on the left and ride sides of the TPM image are due to electrodes boundaries which can be seen in Fig. 2(b), while the narrow line in the middle along the waveguide is attributed to the recorded field. This measurement confirms that charge movement is taking place only in the waveguide core.

The refractive index change at ω_m was measured after electric-field poling without any additional DC field applied on the electrodes. It is found that Δn^p_ω due to the field inscribed by a poling voltage V_p of 400 V is less than Δn^{up}_ω, obtained in the case a DC voltage of equivalent value applied on the electrodes: it is of 94% and 60% for the wide and narrow waveguide, respectively. The values of Δn^{up}_ω and Δn^p_ω are shown in Table 2. The difference in the induced refractive index change, in cases of unpoled waveguide having applied $V_{DC} =$

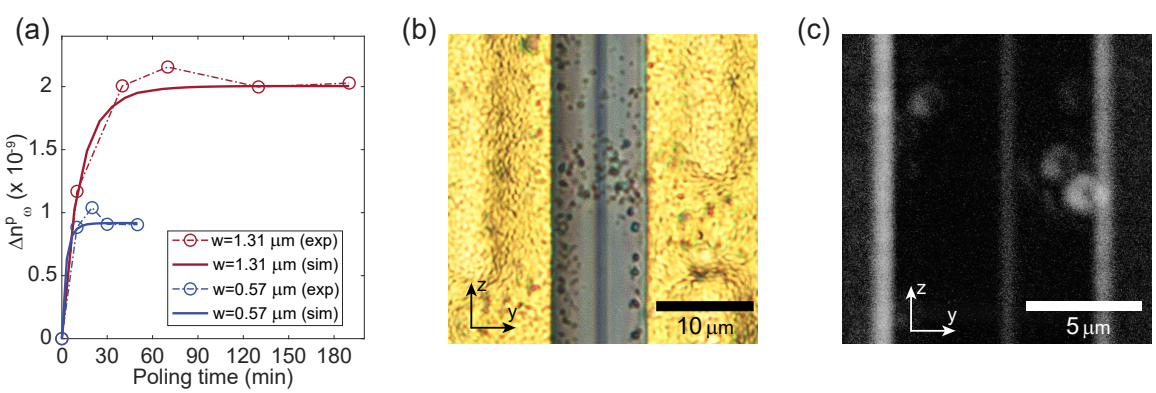

Figure 2. (a) Temporal evolution of the induced refractive index change normalized for $V_m = 1$ V. The hollow circles connected with dash-dotted lines are experimentally obtained values. Solid lines represent simulated dynamics. (b) Optical photograph and (c) TPM image of the narrow after electric-field poling.

Table 2. Refractive index change in the linear regime normalized for $V_m = 1$ V before poling under $V_{DC} = 400$ V (Δn_ω^{up}) and after the poling treatment (Δn_ω^{p}) under $V_p = 400$ V in the wide and narrow waveguides.

Cross-section	Δn_ω^{up} ($V_{DC} = 400$ V)	Δn_ω^{p}
1.31×0.81 μm^2	2.2×10^{-9}	2.0×10^{-9}
0.57×0.81 μm^2	1.5×10^{-9}	0.9×10^{-9}

400 V and poled waveguide with 400 V between the electrodes, can be explained by the overlap of the optical mode with the externally applied or inscribed static electric field before and after poling, respectively. During a poling process, the charges migrate towards one side of the waveguide core, forming a depleted zone. Thus, the inscribed electric field does not extend to the whole waveguide core. Only part of the optical mode interacts with the static electric field leading to the smaller value of the overlap integral. Compared to the core cross-section of the narrow waveguide, the inscribed field covers less area resulting in the smaller overlap integral and refractive index change.

A two-dimensional model describing the formation of an induced space-charge region within a Si_3N_4 waveguide was implemented to simulate the thermally assisted electric field poling dynamics similarly as used elsewhere.[19,20] In the model, we assume that initially, the waveguide is electrically neutral, the process takes place exclusively in a waveguide core, only one mobile charge specimen is involved, and the present charges are uniformly distributed. The actual sign of the mobile charge is unknown, and for the simulation it was chosen to be positive. The charge concentration and the diffusion coefficient were varied to fit the temporal evolution of the induced second-order nonlinearity. We estimated the concentration of the charges of 0.15 mol/m^3 and 0.085 mol/m^3, and the diffusion coefficient of 0.35×10^{-18} m^2/s and 1×10^{-18} m^2/s for the wide and narrow waveguide, respectively. The solid lines in Figure 2(a) represent the refractive index change calculated using the profile of the inscribed field for both waveguides, showing an excellent match with experimental values.

The simulated inscribed electric field profile and the corresponding mobile charge distribution for the studied

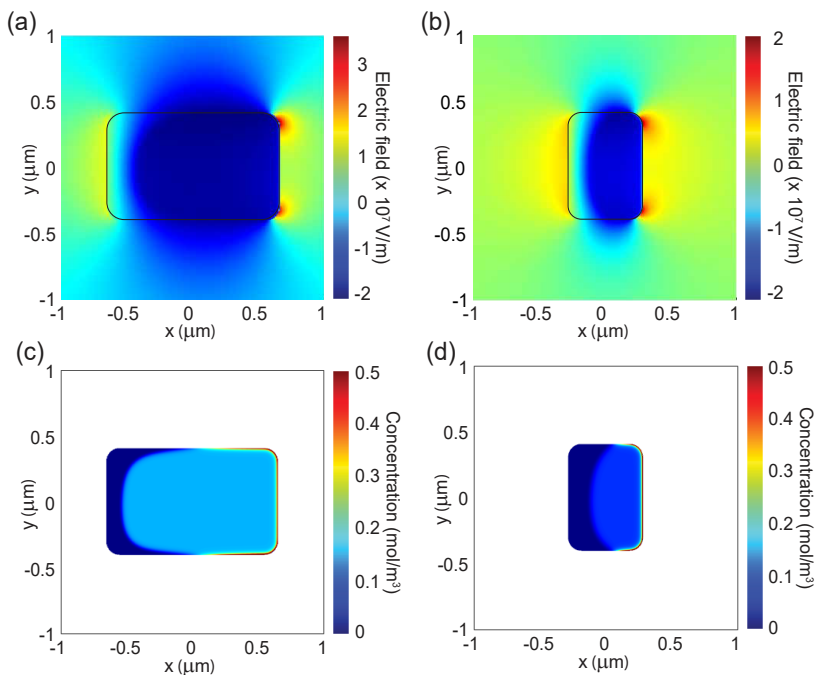

Figure 3. (a, b) Inscribed electric field profiles and (c, d) mobile charge distribution in the waveguides with 1.31 x 0.81 μm^2 and 0.57 x 0.81 μm^2 cross-section, respectively, after electric-field poling.

waveguides are plotted in Fig. 3. The charges traverse some distance to compensate the externally applied field, thus, the recorded field takes only the part of the space in the waveguide core. For the wide waveguide, this distance is almost negligible in comparison with its width, which results in a small change of the overlap integral and, hence, the induced refractive index change (Table 2). In contrast, the significant part of the propagating optical mode in the narrow waveguide does not interact with any static electric field that causes the reduction of the modulation amplitude.

3. CONCLUSIONS

For the first time, we have demonstrated thermally assisted electric-field poling in Si_3N_4 waveguides. The poling process occurs exclusively within the Si_3N_4 waveguide core according to two-photon microscopy images and the developed model describing the induced refractive index change before and after the poling treatment. Using the numerical simulation, we estimated the concentration between 0.085 and 0.15 mol/m^3 and the diffusion coefficient in the range 0.35-1$\times10^{-18}$ m^2/s of the charge responsible for the space-charge electric field formation in Si_3N_4. The dependence of the modulation amplitude after the poling treatment on a waveguide cross-section is described as the change of an overlap between a propagating optical mode and an inscribed field. In addition, the DC third-order susceptibility of Si_3N_4 $\chi^{(3)} = 1.4\times10^{-21}$ pm/V previously unknown in the literature has been measured.

ACKNOWLEDGMENTS

The funding was provided by ERC grant PISSARRO (ERC-2017-CoG 771647).

REFERENCES

[1] Kim, B. Y., Okawachi, Y., Jang, J. K., Yu, M., Ji, X., Zhao, Y., Joshi, C., Lipson, M., and Gaeta, A. L., "Turn-key, high-efficiency kerr comb source," *Opt. Lett.* **44**, 4475–4478 (Sep 2019).

[2] Porcel, M. A. G., Schepers, F., Epping, J. P., Hellwig, T., Hoekman, M., Heideman, R. G., van der Slot, P. J. M., Lee, C. J., Schmidt, R., Bratschitsch, R., Fallnich, C., and Boller, K.-J., "Two-octave spanning supercontinuum generation in stoichiometric silicon nitride waveguides pumped at telecom wavelengths," *Opt. Express* **25**, 1542–1554 (Jan 2017).

[3] Moody, G., Chang, L., Steiner, T. J., and Bowers, J. E., "Chip-scale nonlinear photonics for quantum light generation," *AVS Quantum Science* **2**(4), 041702 (2020).

[4] Chmielak, B., Waldow, M., Matheisen, C., Ripperda, C., Bolten, J., Wahlbrink, T., Nagel, M., Merget, F., and Kurz, H., "Pockels effect based fully integrated, strained silicon electro-optic modulator," *Opt. Express* **19**, 17212–17219 (Aug 2011).

[5] Castellan, C., Trenti, A., Vecchi, C., Marchesini, A., Mancinelli, M., Ghulinyan, M., Pucker, G., and Pavesi, L., "On the origin of second harmonic generation in silicon waveguides with silicon nitride cladding," *Sci. Rep.* **9**(1088), 148–154 (2019).

[6] Billat, A., Grassani, D., Pfeiffer, M. H. P., Kharitonov, S., Kippenberg, T. J., and Brès, C.-S., "Large second harmonic generation enhancement in si_3n_4 waveguides by all-optically induced quasi-phase-matching," *Nat. Commun* **8** (October 2017).

[7] Hickstein, D. D., Carlson, D. R., Mundoor, H., Khurgin, J. B., Srinivasan, K., Westly, D., Kowligy, A., Smalyukh, I. I., Diddams, S. A., and Papp, S. B., "Self-organized nonlinear gratings for ultrafast nanophotonics," *Nat. Photon.* **13**, 494–499 (July 2019).

[8] Nitiss, E., Tianyi Liu, D. G., Pfeiffer, M., Kippenberg, T. J., and Brès, C.-S., "Formation rules and dynamics of photoinduced $\chi^{(2)}$ gratings in silicon nitride waveguides," *ACS Photonics* **7**, 147–153 (January 2020).

[9] Anderson, D. Z., Mizrahi, V., and Sipe, J. E., "Model for second-harmonic generation in glass optical fibers based on asymmetric photoelectron emission from defect sites," *Opt. Lett.* **16**, 796–798 (Jun 1991).

[10] Dianov, E. M. and Starodubov, D. S., "Photoinduced generation of the second harmonic in centrosymmetric media," *Quantum Electronics* **25**, 395–407 (may 1995).

[11] Myers, R. A., Mukherjee, N., and Brueck, S. R. J., "Large second-order nonlinearity in poled fused silica," *Opt. Lett.* **16**, 1732–1734 (Nov 1991).

[12] Alley, T. G., Brueck, S., and Myers, R. A., "Space charge dynamics in thermally poled fused silica," *Journal of Non-Crystalline Solids* **242**(2), 165–176 (1998).

[13] Wong, D., Xu, W., Fleming, S., Janos, M., and Lo, K.-M., "Frozen-in electrical field in thermally poled fibers," *Optical Fiber Technology* **5**(2), 235–241 (1999).

[14] Sze, S. M. and Ng, K. K., [*Physics of semiconductor devices, third edition*], Wiley, 3rd ed. ed. (2006).

[15] Damas, P., Berciano, M., Marcaud, G., Alonso Ramos, C., Marris-Morini, D., Cassan, E., and Vivien, L., "Comprehensive description of the electro-optic effects in strained silicon waveguides," *Journal of Applied Physics* **122**(15), 153105 (2017).

[16] Liu, A. C., Digonnet, M. J. F., and Kino, G. S., "Measurement of the dc kerr and electrostrictive phase modulation in silica," *J. Opt. Soc. Am. B* **18**, 187–194 (Feb 2001).

[17] Ikeda, K., Saperstein, R. E., Alic, N., and Fainman, Y., "Thermal and kerr nonlinear properties of plasma-deposited silicon nitride/silicon dioxide waveguides," *Opt. Express* **16**, 12987–12994 (Aug 2008).

[18] Kudlinski, A., Quiquempois, Y., and Martinelli, G., "Modeling of the $\chi(2)$ susceptibility time-evolution in thermally poled fused silica," *Opt. Express* **13**, 8015–8024 (Oct 2005).

[19] Camara, A., Tarasenko, O., and Margulis, W., "Study of thermally poled fibers with a two-dimensional model," *Opt. Express* **22**, 17700–17715 (Jul 2014).

[20] Lucia, F. D., Bannerman, R., Englebert, N., Velazquez, M. M. A. N., Leo, F., Gates, J., Gorza, S.-P., Sahu, J., and Sazio, P. J. A., "Single is better than double: theoretical and experimental comparison between two thermal poling configurations of optical fibers," *Opt. Express* **27**, 27761–27776 (Sep 2019).